Chapter 3. Simulation model development

3.1. Mathematical modelling of SI engine

3.1.1. Preference for Quasi-dimensional (QD) modelling

Quasi-dimensional thermodynamic modelling (QDTM) is a multizone combustion modelling methodology capable of mimicking the actual thermodynamic state of a closed system by means of considering a suitable flame propagation and heat transfer sub-models [66]. A schematic representation for the two-zone based QD modelling has been depicted in Figure 3.1.1. Several authors have utilized the quasi-dimensional thermodynamic model method for engine performance depiction (e.g. [66],[171, 172],[64]). QDTM applies fundamental thermodynamic-based energy and mass conservation models, thus requiring the thermochemical properties and net calorific values of induced fuel-blend definition [46, 173]. Table 3.1 presents the ASTM-standard mixture properties referenced from- [49] and [26].

Table 3.1: Properties of sewage sludge producer gas–methane blends

Fuel	**Fuel composition by V%**	**Calorific Value (MJ/kg)**	**Reference**
Sewage sludge Producer gas (SSPG)	H_2: 13% CO: 16% CH_4: 3% CO_2: 15% N_2: 53% Density: 1.1 kg/m^3	4.05	[26], [49]
Methane	CH_4:100%	50.33	[49]
SSPG10	10% SSPG+90% methane	42.82	Calculated
SSPG25	25% SSPG+75% methane	35.59	
SSPG50	50% SSPG+50% methane	21.28	
SSPG75	75% SSPG+25% methane	11.70	
SSPG90	90% SSPG+10% methane	6.92	

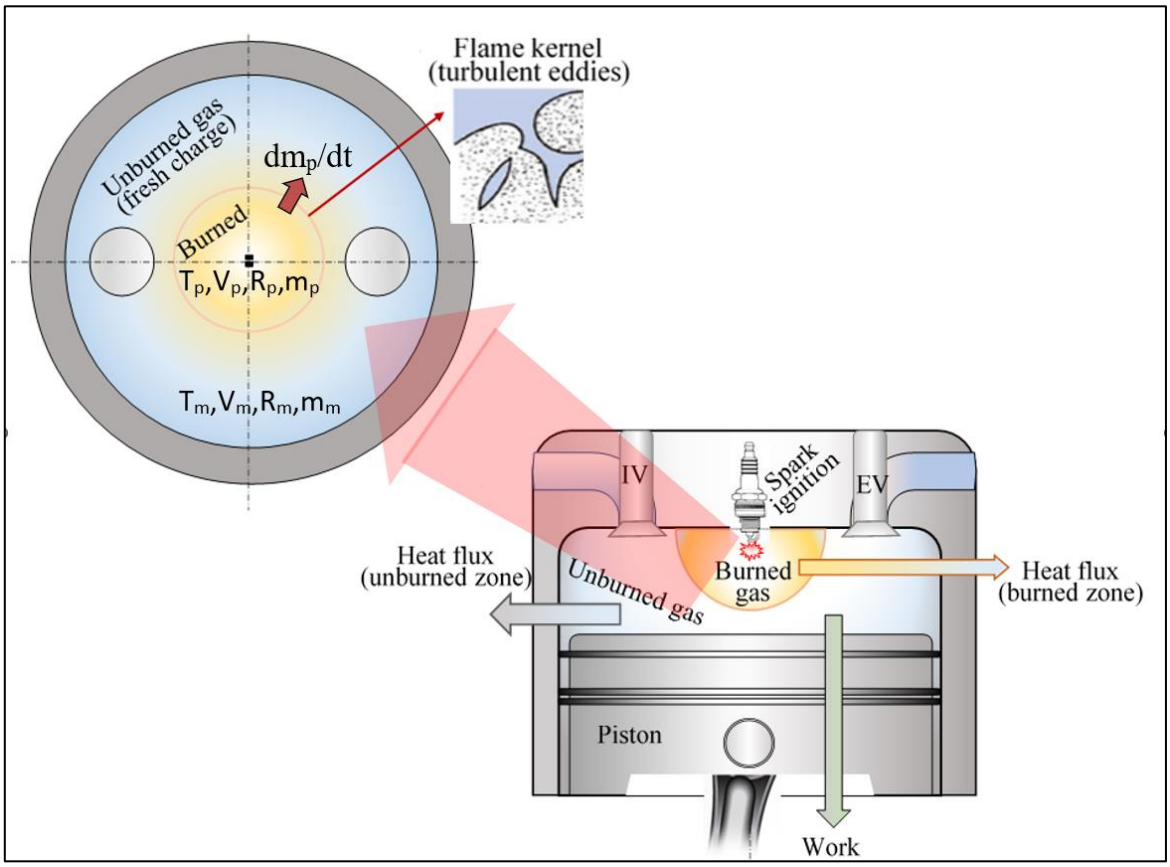

Figure 3.1.1. Two-zone combustion modelling schematic

3.1.2. QDTM: assumptions, modelling

Considering the open and closed combustion systems, the power-cycle phase of IC engine systems is significant. The power cycle is considered to initiate with Inlet valve closure (IVC). Modelling the power cycle enables analyzing the engine performance characteristics [64]. As the power cycle begins from the inlet valve close and extends until the exhaust valve opens, its modelling is conventionally implemented in the three phase-approach. These modes are each affiliated with single-zone compression, two-zone combustion, and single-zone expansion phases [174]. QDTM has been applied in this study to model the power cycle and simulate the performance and emission outcomes. A schematic layout for the programmed QDTM-based

simulation approach is shown in Figure 3.1.2. The FORTRAN-coded model is programmed to simulate the SI engine having the specifications depicted in Table 3.2. The mathematical expressions that governed the QDM-based simulation are discussed in this manuscript. Two-zone combustion modelling is programmed to incept with spark. Ignition takes effect when the flame kernel grows more than 0.01 times of in-cylinder volume and thus accounts for the ignition delay [175, 176]. For streamlining calculations, this model included an array of assumptions, like:

- induced air-fuel charge behaves like a homogeneous ideal gas with uniform local specific heat
- burned and unburned zones incept with flame kernel formation
- no heat transfers via the two-zone boundaries
- inside pressure of the cylinder is uniform at all times
- combustion terminates with charge volume induction reducing to zero
- excluding CO, NO, the twelve burned gas compositions (H, H_2, OH, H_2O, CO, CO, CO_2, O, O_2, N, N_2, NO, and Ar) exhibit thermodynamic equilibrium
- A simpler spherical flame front is considered for the modelling.
- The subsequent combustion propagation is assumed to have turbulent flame speed, infinitesimal thickness, and spherical flame front.

The flame front is considered to separate the two zones: burned and unburned zones. The "burned zone" is immediately adjacent to the spark, and the "unburned zone" is ahead of the flame front. The unburned zone consists of fresh gaseous fuel and air mixture, whereas the burned zone consists of combustion products[46].

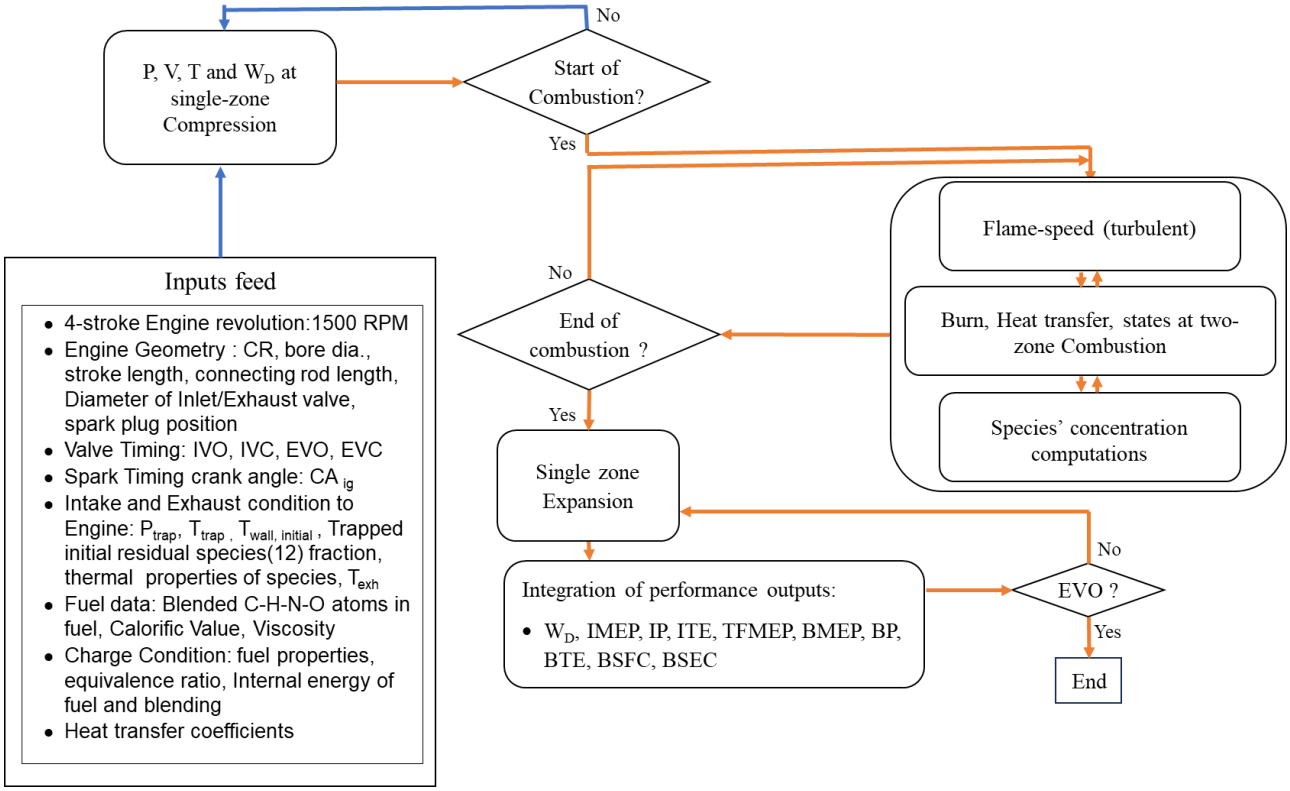

Figure 3.1.2. Process layout for the simulation

Table 3.2: Engine specifications particular to the simulation

Particulars	**Engine Specification**
Engine model	Wiscon TM27, freely aspirated [65]
Engine type	4 Stroke-Spark Ignition Engine
Bore Diameter (mm)	91.0
Compression ratio (r)	12
Stroke (mm)	103.2
Connecting rod span (mm)	136.5
Start of ignition (crank angle)	30-45 BTDC *(variable)*
Equivalence ratio	0.8
PG fraction to methane, by volume%	25-75% *(variable)*
Inlet-valve close	50º-90º ABDC *(variable)*
RPM	1500

The flame front geometry governs the mass and volume fractions whereas burned gas composition is further calculated utilizing the equilibrium algorithms. The unstable concentrations of CO and NO are additionally computed using the rate kinetic model approach[177, 178]. Fourth-order Runge-Kutta method is employed to solve the differential equations that model varying thermodynamic states of combustion respective to crank angle variation. The Newton-Raphson method is employed to fetch the final product species concentration calculation. During the power cycle, net-heat transfer with cylinder walls is also formalized using Annand's correlation[179].

Conservation of energy and mass-based thermodynamic correlations are used to model the power cycle. The model is implemented considering fixed speed operation of 1500 RPM and programmed for three consecutive phases in each simulation iteration. The phases are single-zone compression, then quasi-dimensional two-zone combustion, and again a single-zone expansion.

3.1.2.1. Compression modelling

3.1.2.1.1. In-cylinder pressure modelling

Expressions 1 and 2 govern the in-cylinder single-zone temperature and pressure variations corresponding to the crank angles during the compression and expansion phases.

$$\frac{dT_m}{d\theta} = T_m\left(\frac{1}{V}\frac{dV}{d\theta} + \frac{1}{P}\frac{dP}{d\theta}\right) \tag{1}$$

$$\frac{dP}{d\theta} = \left(\frac{1}{V}\right)\left[\left(\frac{R}{c_v}\right)\left(\frac{dQ}{d\theta}\right) - \left(\frac{PdV}{d\theta}\right)\left(\frac{R}{c_v}+1\right)\right] \tag{2}$$

Here, $dT_m/d\theta$ represents the temperature differential of the unburned mixture and $dP/d\theta$ represents the chamber-pressure differential, where P remains uniform at any instantaneous crank angle(θ)[55]. The application of such approaches is also verified in ref.-[60, 110] as well.

V is the instantaneous cylinder volume in terms of the θ (obtainable in equation (3), and its differential is also depicted through expression (4) [177].

$$\frac{dV}{d\theta} = \frac{V_c}{2}(CR-1)\left[(\sin\theta) + \frac{\sin\theta\cos\theta}{\sqrt{\frac{L^2}{a_c^{\,2}} - \sin^2\theta}}\right] \tag{3}$$

$$V = \frac{\pi}{4}D^2 a_c\left[(1-\cos\theta) + \frac{L}{a_c} - \sqrt{\frac{L^2}{a_c^{\,2}} - \sin^2\theta}\right] \tag{4}$$

The work produced at the piston is assessed using the differential in equation (5).

$$\frac{dW}{d\theta} = p\frac{dV}{d\theta} \tag{5}$$

The pressure and temperature variations at the two-zone combustion are typically modelled utilizing the differential equations: (6-8). Here, the suffix ‘m’ and ‘p’ refer to unburnt fuel-air charge and combustion products, respectively. The iterative Fourth-order Runge-Kutta model solves these differential equations. Complete derivations for these utilized equations are further presented in the appendix (Eqn.1-14).

$$\frac{dT_m}{d\theta} = \frac{1}{m_m c_{P,m}}\frac{dQ_m}{d\theta} + \frac{V_m}{m_m c_{P,m}}\frac{dP}{d\theta} \tag{6}$$

$$\frac{dT_p}{d\theta} = \frac{P}{m_p R_p}\left[\frac{dV}{d\theta} - \left(\frac{R_p T_p}{P} - \frac{R_m T_m}{P}\right)\frac{dm_p}{d\theta} - \frac{R_m}{c_{p,m}P}\frac{dQ_m}{d\theta} - \frac{R_m V_m}{c_{p,m}P}\frac{dP}{d\theta} + \frac{V}{P}\frac{dP}{d\theta}\right] \tag{7}$$

$$\frac{dP}{d\theta} = \frac{\left(1+\frac{c_{v,p}}{R_p}\right)P\frac{dV}{d\theta} + \left(\frac{c_{v,m}}{c_{P,m}} - \frac{c_{v,p}R_m}{R_p c_{p,m}}\right)\frac{dQ_m}{d\theta} + \left[\left(e_p - e_m\right) - c_{v,p}\left(T_p - \frac{R_m T_m}{R_p}\right)\right]\frac{dm_p}{d\theta} - \frac{dQ}{d\theta}}{\left(\frac{c_{v,m}V_m}{c_{P,m}} - \frac{c_{v,p}}{R_p}\frac{R_m V_m}{c_{p,m}} + \frac{c_{v,p}V}{R_p}\right)} \tag{8}$$

3.1.2.2. Two-zone combustion and sub-models

Unlike the zero-dimensional model, the two-zone quasi-dimensional model is capable of assessing flame propagation by considering the spatial distribution of flame and rate of burn. However, the two-zone model disregards the complicated structure and thickness of the flame front, as regarded in the multi-zone models. It considers only the flame-front position and shape [65]. The Schematic for the combustion model was illustrated in Figure 3.1.1.

3.1.2.2.1. Burn rate entrainment and corresponding thermodynamic state

The rate of burn (dm_p/dt) is dependent on the flame speed and is calculated from the geometry of the burned zone inside the combustion chamber. The burn rate is expressed in equation 9, where u_t represents turbulent flame-front speed, and A_f represents the flame-front area.

$$\frac{dm_p}{dt} = \frac{-dm_m}{dt} = \rho_m u_t A_f \tag{9}$$

Considering the ideal gas nature in a two-zone combustion model the differential of induced charge volume respective to θ-variations is presented in equation 10, where the suffix '*ch*' represents the flame front-induced charge.

$$\frac{dV_{ch}}{d\theta} = \frac{dV_m}{d\theta} + \frac{dV_p}{d\theta} = \left(\frac{V_p}{m_p} - \frac{V_m}{m_m}\right)\frac{dm_p}{d\theta} + \frac{m_m R_m dT_m}{p}\frac{dT_m}{d\theta} + \frac{m_p R_p dT_p}{p}\frac{dT_p}{d\theta} - \frac{Vdp}{pd\theta} \tag{10}$$

Referring to equation 11, the thermodynamic mass and energy conservation principle is modelled to track the combustion progress by utilizing equation 11, where the differential of net internal energy, work output, and heat transfer for the closed volume is indicated respectively to θ-variations. Here, e_p and e_m represent the specific internal energy. c_{vp} and c_{vm} are specific heats of two-zone mixtures, calculated by polynomial coefficients as depicted in Ref.-[110, 180]. The models for internal energy, specific heats, and reaction enthalpy sub-models have been further detailed in the supplementary file equation 12-17.

$$\left\{\left(e_p - e_m\right)\frac{dm_p}{d\theta} + m_m c_{vm}\frac{dT_m}{d\theta} + m_m c_{vp}\frac{dT_p}{d\theta}\right\} + \left\{p\frac{dV_{ch}}{d\theta}\right\} - \left\{\frac{dQ}{d\theta}\right\} = 0 \tag{11}$$

Specific heat and internal energy for the exhaust species and air are modelled as per the following equations:(12 to 14). The polynomial coefficients, as: a_i (i = 1, 2, 3, 4, 5, 6), were considered from the ref-[180], and used for this modelling. The modelling values are also further listed in Table 3.3.

$$c_v = (a_1 - 1)\bar{R} + (a_2 T + a_3 T^2 + a_4 T^3 + a_5 T^4)\bar{R}\ \left(\text{J}/\text{mol-K}\right) \tag{12}$$

$$\bar{h} = \left(a_1 T + \frac{a_2}{2}T^2 + \frac{a_3}{3}T^3 + \frac{a_4}{4}T^4 + \frac{a_5}{5}T^5 + a_5\right)\bar{R}\left(\text{J}/\text{mol}\right) \tag{13}$$

$$\bar{u} = \left(\left(a_1 - 1\right)T + \frac{a_2}{2}T^2 + \frac{a_3}{3}T^3 + \frac{a_4}{4}T^4 + \frac{a_5}{5}T^5 + a_5\right)\bar{R}\ \left(\text{J}/\text{mol}\right)$$

$$\Rightarrow \bar{u}(T) = u_1 + u_2 T + u_3 T^2 + u_4 T^3 + u_5 T^4 + u_6 T^5\ \left(\text{J}/\text{mol}\right) \tag{14}$$

Table 3.3: Value of the constants

$\bar{u}(T)$ Polynomial coefficients for :	
PG	**CH_4**
$u_1 = -488.4 \times 10^5$	$u_1 = -0.764 \times 10^8$
$u_2 = 20050.34$	$u_2 = -14.532 \times 10^3$
$u_3 = 1.4081$	$u_3 = 154.79$
$u_4 = 5.2013 \times 10^{-3}$	$u_4 = 0.0601$
$u_5 = 1.69897 \times 10^{-6}$	$u_5 = 8.387 \times 10^{-6}$
$u_6 = -1.3983 \times 10^7$	$u_6 = 49.54 \times 10^6$

Access to the thermodynamic properties of the fuel is modelled by utilizing the approach presented in ref-[110] and depicted in equations- (15 to 17), where *h* and *e* represent specific-

enthalpy and total internal energy, respectively. Further, pV is the representation for work conversion from the fuel and the included constants represent the polynomial coefficients as revealed in John.et.al [180]. The polynomial coefficients as: A_i (i = 1, 2, 3, 4, 5, 6), from the ref-[180] were used for this modelling.

$$\overline{h_f} = \overline{e_f} + p\overline{V} = A_{f1}t + \frac{A_{f2}t^2}{2} + \frac{A_{f3}t^3}{3} + \frac{A_{f4}t^4}{4} - \frac{A_{f5}}{t} + A_{f6} + A_{f8} \left(\text{kCal}/\text{kmol}\right) \quad (15)$$

$$\overline{e_f} = \frac{(A_{f1} - \overline{R})T}{1000} + \frac{A_{f2}t^2}{2.(1000)^2} + \frac{A_{f3}t^3}{3.(1000)^3} + \frac{A_{f4}t^4}{4.(1000)^4} + A_{f6} + A_{f8} - A_{f5} * \frac{1000}{T} \quad (16)$$

A_{f6} and A_{f8} represent enthalpy content at 298.15 K, and its supplementary at T.

$$\Rightarrow \overline{e_f}(T) = \left[\alpha_{f1} + \alpha_{f2}T + \alpha_{f3}T^2 + \alpha_{f4}T^3 + \alpha_{f5}T^4 + \alpha_{f5}T^5 + \alpha_{f6}T^{-1}\right] \left(\text{J}/kmol\right) \quad (17)$$

Thus, $\alpha_{f1} = \left[A_{f6} + A_{f8}\right] \times 4184 \times 10^3$ (J/kmol), $\alpha_{f2} = \left[\frac{(A_{f1} \times 4184 \times 10^3)}{1000} - -\overline{R}\right]$,

$\alpha_{f3} = \left[\frac{A_{f2}}{2.(1000)^2}\right] \times 4184 \times 10^3$, $\alpha_{f4} = \left[\frac{A_{f3}}{3.(1000)^3}\right] \times 4184 \times 10^3$, $\alpha_{f5} = \left[\frac{A_{f4}}{4.(1000)^4}\right] \times 4184 \times 10^3$,

$\alpha_{f6} = \left[A_{f5} \times 10^3\right] \times 4184 \times 10^3$.

Annand's equation was used to assess the heat transfer rate from gas to adjacent walls considering the convective and radiant heat transfer components[181]. It was modelled using equation 18 as in ref-[175], where F, d, R_e, K_q, T_m, and T_w are cylinder wall area, bore diameter, Reynold's number, thermal conductivity, product, and wall temperature, respectively. The constants were considered as a=0.4, b=0.7, c=-4.3 x 10^{-9} as per ref-[110, 175].

$$\frac{q_h}{F} = \frac{aK_q}{d}\left(\text{Re}\right)^b (T_m - T_w) + c(T_m^4 - T_w^4) \quad (18)$$

Following the ignition delay, the two-zone burning is modelled to affect the thermodynamic states[176]. The change in temperature and pressure states were governed by the derived differential equations respective to the variations in crank-angle (α, during combustion) as presented below (equations- 19 to 21), by referring-[171, 172, 182]:

$$\frac{dT_m}{d\alpha} = \frac{V_m}{m_m C_{p_m}}\left(\frac{dP}{d\alpha}\right) + \left(\frac{1}{m_m C_{p_m}}\right)\left(\frac{dQ_m}{d\alpha}\right) \tag{19}$$

$$\frac{dT_p}{d\alpha} = \frac{p}{m_p R_p}\left[\frac{dV}{d\alpha} - \left(\frac{R_p T_p}{p} - \frac{R_m T_m}{p}\right)\frac{dm_p}{d\alpha} - \frac{R_m V_m}{p c_{p_m}}\frac{dp}{d\alpha} - \frac{R_m}{p c_{p_m}}\frac{dQ_m}{d\alpha} + \frac{V dp}{p d\alpha}\right] \tag{20}$$

$$\frac{dp}{d\alpha} = \frac{\left(1+\frac{c_{v_m}}{R_p}\right)p\frac{dV}{d\alpha} + \left\{\left(u_p - u_m\right) - c_{v_p}\left(T_p - \frac{R_m}{R_p}T_m\right)\right\}\frac{dm_p}{d\alpha} + \left\{\frac{c_{v_m}}{c_{p_m}} - \frac{c_{v_p}}{R_p}\frac{R_m}{c_{p_m}}\right\}\frac{dQ_m}{d\alpha} - \frac{dQ}{d\alpha}}{\left[\frac{c_{v_p}}{c_{p_m}}\frac{R_m}{R_p}V_m - \frac{c_{v_m}}{c_{p_m}}V_m - \frac{c_{v_p}}{R_p}V\right]} \tag{21}$$

3.1.2.2.2. Flame front geometry and velocity

In modelling, the flame speed of specific fuel blends is calculated using Le Chatelier's Rule. As depicted in the Figure 3.1.1, a spherical-shaped flame-front geometry is adopted in the simulation model. This is because, a spherical flame-front geometry has been identified to effectively simulate the actual outcomes in many reference works[46, 66].

The utilized turbulent flame speed(u_t) is a summation of turbulent intensity (u') and empirical-based laminar flame speed ($S_{L;(PG+CH4)}$). Expressions (22) and (23) present the formulations for approximating u_t and u′, respectively. Flame propagation speed (laminar) for propane (S_{L-PG})[183] and methane (S_{L-CH_4})[184] are measured in m/s, with '*x*' representing the molar fraction

of propane in the fuel intake. Le Chatelier's Rule was utilized in formulating the laminar flame speeds of PG and methane blends in terms of mixture equivalence ratio (ϕ), the molar fraction of PG (x), and reduced temperature and pressure of the combustion chamber. Similar approaches in calculating the laminar flame speeds have been verified by many authors [182, 185]. Equations (24), (25), and (26) respectively present the formulation for laminar flame speeds of PG, methane, and the blends by considering reference temperature (T_o) and pressure (P_o) as 300 K, 101.325 kPa, respectively, as also done in ref-[175]. Further, S_{l0}, α_T, and β_P are calibration constants considered as per Table 3.4.

$$u_t = u' + S_{L-(PG+CH_4)} \tag{22}$$

$$u' = 0.55 S_p \left[1 - \frac{0.5(\theta - 180)}{45} \right] \tag{23}$$

$$S_{L-PG} = (S_{l0})_{PG} \left(\frac{T_m}{T_o} \right)^{\alpha_T} \left(\frac{P_m}{P_o} \right)^{\beta_p} \tag{24}$$

$$S_{L-CH_4} = (S_{l0})_{CH_4} \left(\frac{T_m}{T_o} \right)^{\alpha_T} \left(\frac{P_m}{P_o} \right)^{\beta_p} \tag{25}$$

$$S_{L(PG-CH_4)}(\phi, T, P, x) = \frac{1}{\frac{x}{S_{L-PG}(\phi, T, P)} + \frac{1-x}{S_{L-CH_4}(\phi, P, T)}} \tag{26}$$

Table 3.4: Constants to compute flame speed[110]

Constant	Methane gas (value)	PG (value)
S_{l0}	$-177.43\phi^3 + 340.77\phi^2 - 123.66\phi - 0.0097$	$0.56 - 0.827(Ø - 1.186)^2$
α_T	$5.75\phi^2 - 12.15\phi + 7.98$	2.0

β_P	$-0.925\phi^2 + 2\phi - 1.473$	-0.4

3.1.2.2.3. Wall heat transfer modelling

Annand's Heat-transfer model assessed the heat transfer to adjacent walls from the gas in the combustion chamber. Ref.-[181] incorporates a satisfactory implementation for the model towards an auxiliary wall heat-transfer analysis. The governing equation for this numerical model is equation (27), where the constants a, b, and c are considered as 0.4, 0.7, and -4.3 x 10^{-9}, respectively in reference to the investigations of Ref.-[110, 175]. The notations F, R_e, K_q, d, T_w, and T_m are the cylinder wall area, Reynold's number, thermal conductivity, bore diameter, and wall, and gas mixture temperature, respectively.

$$\frac{q_h}{F} = \frac{aK_q}{d}\left(Re\right)^b (T_m - T_w) + c(T_m^4 - T_w^4) \tag{27}$$

3.1.2.3. Combustion Kinetics and Species Formation

The combustion process is modelled to commence with the end of ignition delay [175]. Modelling the emissions has been a significant design aspect for the IC SI engines. Products from the complete combustion get severely dissociated at the high temperatures of the combustion chamber [175]. Thus, additional species are created. Heywood [180] asserted that the concept of chemical equilibrium is valid for predicting high-temperature combustion products. Thus the quasi-dimensional modelling is coupled with the chemical kinetics and equilibrium principles to assess the variations in NO and CO formations as emissions.

The primary chemical reaction model corresponding to one mole of the products is presented in equation (28). Chemical balancing was applied by considering the chemical kinetics to

determine burned gas' that included 12 species. Correspondingly, thirteen non-linear equations, as presented in Equation 29, were solved utilizing the iterative Newton-Raphson method, as proposed by Benson [171, 172]. In equation (28,29), *a* represents moles of fuel for a single mole of products. *x*, *y*, *z,* and *v*, *w* represent the moles of Hydrogen, Oxygen, Nitrogen, and Argon, Carbon, respectively. Here, f_{PG} represented the molar fraction of the PG in the intake fuel-blend, ϕ represented the equivalence ratio of the air-fuel mixture, and the factor *a* scaled inputs as per unit mole of the outputs. Molar outcomes are specific to one-mole the fuel. *X* represents a thermodynamic state variable, which is numerically integrated by fourth ordered Runge-Kutta methodology (expression 30).

$$a\left[\left(1-x_{PG}\right)CH_4+f_{PG}PG\right]+\frac{a}{\phi}\left[2\left(1-x_{PG}\right)+x_{PG}\right]\left(O_2+\frac{78}{21}N_2+\frac{1}{21}Ar\right)\rightarrow\sum_{i=1}^{12}x_i \quad (28)$$

$$X_{Ar}=a.v;\ X_{CO_2}+X_{CO}=a.w;\ 2X_{H_2O}+2X_{H_2}+X_{OH}=a.x;\ X_{H_2O}+X_{OH}+X_{NO}+2X_{CO_2}+X_{CO}+2X_{O_2}+X_O=a.y\ ;2X_{N_2}+X_{NO}+X_N=a.z \quad (29)$$

$$X_{n+1}=X_n+\frac{dX}{d\alpha}\Delta\alpha \quad (30)$$

Associated with equation (28), seven chemical dissociation equations are implemented under the principles of chemical kinetics, as in expression (20). Further, the equilibrium state is governed by: $\left(dG\right)_{T,p}=0$, wherein the equations: (29,30,31) determine the specific Gibb's function, In equation (32), k_g, e_g, d_g, c_g, b_g, and a_g are constants. K_p is the equilibrium constant, which is determined by finding the roots in equations (33) and (34), where x,υ represents the molar fraction, and stoichiometric coefficient, respectively and p represents the uniform pressure.

$$\frac{1}{2}H_2\rightleftharpoons H\ ;\frac{1}{2}O_2\rightleftharpoons O\ ;\frac{1}{2}N_2\rightleftharpoons N\ ;2H_2O\rightleftharpoons 2H_2+O_2\ ;H_2O\rightleftharpoons OH+\frac{1}{2}H_2\ ;CO_2+H_2\rightleftharpoons H_2O+CO\ ;H_2O+\frac{1}{2}N_2\rightleftharpoons H_2+NO \quad (31)$$

$$\frac{g(T)}{\bar{R}T} = a_g(1-lnT) - b_g T - \frac{c_g}{2}T^2 - \frac{d_g}{3}T^3 - \frac{e_g}{4}T^4 - k_g \tag{32}$$

$$\upsilon_a A + \upsilon_a B \rightleftharpoons \upsilon_c C + \upsilon_d D\,; \quad K_p = \frac{x_c^{\upsilon_c} x_d^{\upsilon_d}}{x_a^{\upsilon_a} x_b^{\upsilon_b}} * P^{\upsilon_{c+}\upsilon_d - \upsilon_a - \upsilon_b} \tag{33}$$

$$lnK_p = \left[\sum\left\{\frac{\upsilon.g(T)}{\bar{R}T}\right\}_{\text{Reactant}} - \sum\left\{\frac{\upsilon.g(T)}{\bar{R}T}\right\}_{\text{Product}}\right] - \frac{\Delta H_0}{\bar{R}T} \tag{34}$$

The rate kinetic model determines NO and CO concentrations as they characterize the non-equilibrium nature[180]. Following the reports from Rao et al. [186], extended Zeldovich reaction principle modelled NO concentration, by including chemical reactions shown in Table 3.5.

Table 3.5: Equations for NO-emission, with rate constants

Reactions for NO formation	Associated Forward rate constant
$N + NO \rightleftharpoons N_2 + O$	$K_{1f} = 3.1*10^{10} * e^{(-160/T)}$
$N + O_2 \rightleftharpoons NO + O$	$K_{2f} = 6.4*10^{6} * T * e^{(-3125/T)}$
$N + OH \rightleftharpoons NO + H$	$K_{3f} = 4.2*10^{10}$
$H + N_2O \rightleftharpoons N_2 + OH$	$K_{4f} = 3.0*10^{10} * e^{(-5350/T)}$
$O + N_2O \rightleftharpoons N_2 + O_2$	$K_{5f} = 3.2*10^{12} * T * e^{(-18900/T)}$
$O + N_2O \rightleftharpoons NO + NO$	$K_{6f} = K_{5f}$
$N_2O + M \rightleftharpoons N_2 + O + M$	$K_{7f} = 10^{12} * e^{(-30500/T)}$

NO concentration was calculated using Equation (35) using the Table 3.5 rate constants. In equation (35), $\alpha_e = \frac{[NO]}{[NO]_e}$, where *e* is the equilibrium condition, and $R_1 \sim R_7$ are the equilibrium rates. References-[171, 172] detail the solution descriptions for this utilized method.

$$\frac{1}{V}\frac{d}{dt}\left[\left[NO\right]V\right]=2\left(1-\alpha_e^2\right)\left[\frac{R_1}{1+\alpha_e\frac{R_1}{R_2+R_3}}+\frac{R_6}{1+\frac{R_6}{R_4+R_5+R_7}}\right] \quad (35)$$

The rate kinetic model described by Horlock, Benson, and Baruah [171, 172, 176] was used to calculate CO concentration, with concerned governing chemical equations in equation (36,37).

$$CO+OH \underset{k_b}{\overset{k_f}{\rightleftharpoons}} CO_2+H \quad ; \quad CO+O_2 \underset{k_b}{\overset{k_f}{\rightleftharpoons}} CO_2+O \quad (36)$$

$$\frac{1}{V}\frac{d}{dt}\left[\left[CO\right]V\right]=-k_f[CO2][OH]+k_b[CO2][H] \quad (37)$$

After the peak CO concentration is attained at equilibrium, the temperature declines during expansion and the formulated CO value lags behind equilibrium. Thus, the "COFAC" value is utilized to resolve the originated deviation in simulation. It is calibrated as 0.5, which effectively validates the actual CO concentration. The associated correlation is expressed as equation (38), where XCO is corrected CO, XCO_{eq} is the equilibrium CO value and XCO_{max} represents peak equilibrium CO concentration. The COFAC factor scales XCO to actual by calibrating it between 0 and 1.

$$XCO = COFAC\ (XCO_{max} - X\ CO_{eq}) + XCO_{eq} \quad (38)$$

Similar to the approach of modelling the SSPG-methane intake as a net fuel blend, the governing thermo-chemical reaction for the Propane-PG dual-fuel combustion with air is modelled for a single mole of net product. Equation-39 reflects this chemical equation, where *'f'* denotes the mole percentage of Propane (C_3H_8) in the fuel composition. Following this oxidization, the concentrations of 12 burned-gas species are calculated using fundamental atomic balancing equations mentioned by Benson et al.[45, 149]. However, because the generation of NO and CO is a non-equilibrium process, the Rate kinetic model is used to

simulate the NO and CO concentrations, as suggested by Lavoie et al.[54, 149] and J. H. Horlock et al.[21, 28]. Further information on model expressions involved in computing blended LHVs, inter-relations between mole fraction (*f*) and a mass fraction (*x*), blended Molecular Elementary concentrations as: $x.(u_i)_{C_3H_8}+(1-x)(u_i)_{PG}$, and blend fraction designations for propane blends are depicted in Table 3.6.

$$a\left[\left(f_{C_3H_8}\right)C_3H_8+\left(1-f_{C_3H_8}\right)PG\right]+\frac{a}{\varphi}\left[2\left(f_{C_3H_8}\right)+\left(1-f_{C_3H_8}\right)\right]\left(O_2+\frac{78}{21}N_2+\frac{1}{21}Ar\right)\rightarrow\sum_{i=1}^{12}x_i \quad (39)$$

Dual fuel composition for (x) (Propane gas) + (1-x) (Producer gas), is mentioned in Table 3.6, where x is the mass fraction of Propane in the fuel mixture.

Table 3.6. Depiction of C-H-N-O atoms in the Propane-Grape PG mixture

Element	**Value**
C-atom	3-2.75x
H-atom	8-7.55x
N-atom	1.278x
O-atom	0.2898x
Blended LHV (MJ/kg)	$x.LHV_{C_3H_8}+(1-x)LHV_{PG}$
Relation between mole fraction (*f*) and mass fraction (*x*) [187]	here, $x=\frac{f.MW_{C_3H_8}}{f.MW_{C_3H_8}+(1-f)MW_{PG}}$
Blended Molecular Weight (g/mol)	*x44.1+(1-x)23.877*
Coefficient of blended polynomial coefficient	$x.(u_i)_{C_3H_8}+(1-x)(u_i)_{PG}$
Volume % of blendings	**representations**
20% propane+80% Producer gas	B20
40% propane+60% Producer gas	B40
60% propane+40% Producer gas	B60
80% propane+20% Producer gas	B80

3.1.2.4. Single-zone expansion

The power cycle extends from IVC to EVO. Thus, a portion of the expansion is modelled with a single zone. The single zone is modelled to consist of the residual products of the combustion. The thermodynamic state inside the combustion chamber is assessed in a similar fashion as in the compression.

3.1.2.5. Formulations for performance parameters

The equivalence ratio (ϕ, ER), is the mass ratio of theoretical air needed for complete combustion of the intake fuel to the actual air volume in the cylinder [188]. It is set to lean (0.8) for all the analyses carried out in this investigation. Equation 40 expresses the ER for the considered dual-fuel input.

$$\phi = \frac{m_{CH_4}\left(kg/s\right).\phi_{stoic,CH_4} + m_{PG}\left(kg/s\right).\phi_{stoic,PG}}{V_m\left(m^3\right)} \tag{40}$$

The performance output algorithms were formulated as per the following sequenced correlations (Equations 41-51)

Indicated work: $$\frac{dw}{d\alpha} = p\frac{dV}{d\alpha}\ , \quad W_d = \int_{IVC}^{EVO}\left\{P\ \theta\ .\frac{dV}{d\theta}\right\}d\theta \tag{41}$$

Indicated mean effective pressure: $$IMEP\ (bar) = \frac{W_d(kJ)/100}{V(m^3)} \tag{42}$$

Indicated Power: $$IP\ (kW) = \frac{W_d(kJ)}{120}N\ \ ;\ N \text{ is rpm} \tag{43}$$

Indicated thermal efficiency : $$ITE = \frac{IP(kW)}{m\ kg/s\ .CV\ kg} \tag{44}$$

Indicated Specific fuel consumption: $$ISFC\ \ kg/kWh = \frac{3600}{\eta_{ith} CV\ kJ/kg} \tag{45}$$

Overall/Total friction mean-effective pressure (TFMEP) [180]:

$$\mathrm{TFMEP(bar)} = 0.97 + 0.15\left(\frac{\mathrm{N}}{1000}\right) + 0.05\left(\frac{\mathrm{N}}{1000}\right)^2 \quad (46)$$

Brake mean effective pressure : $\mathrm{BMEP} = \mathrm{IMEP} - \mathrm{TFMEP}$ (47)

Brake Power: $\mathrm{BP(kW)} = \frac{\mathrm{BMEP}.V_S.\mathrm{N}}{120}$ (48)

Brake thermal efficiency: $\mathrm{BTE} = \frac{\mathrm{BP(kW)}}{m_f \ \mathrm{kg/s} \ .\mathrm{CV} \ \mathrm{kJ/kg}}$ (49)

Brake-specific fuel consumption: $\mathrm{BSFC} = \frac{m_f \ \mathrm{kg/s} \ .3600 \ \mathrm{s/hr}}{\mathrm{BP(kW)}}$ (50)

Brake-specific energy consumption[189]: $\mathrm{BSEC} = \mathrm{BSFC} \ \mathrm{kg/kWh} \ .\mathrm{CV} \ \mathrm{kJ/kg}$ (51)

For the initial engine response simulation study, the performance and emission parameters of an SI engine fuelled with methane (CH4), and producer gas running at 1500 RPM, were simulated using a FORTRAN-based computational algorithm for varying PG blends. Outcomes are analyzed using an ANOVA-based regression model, followed by RSM-based optimization.

3.2. Statistical Prediction model

The simulation model is firstly coded through a FORTRAN-based program and is run iteratively as per the RSM-based design matrix framework. The QDTM model was also iteratively applied with the inputs set as per the organized design matrix. The simulation-resulted data table is depicted in the results with this organized design matrix arrangement. RSM utilizes this data to correlate the responses with respective independent factors by establishing fitting coefficients for the empirical polynomial regression models [190]. Multi-objective optimization was enabled through RSM to predict the best operative parameters when

the DF mode SI engine model integrated boosted intake and Miller cycle strategies. 'Design Expert-13' software was used to execute this multi-objective optimization. Sets of QDTM simulation input framework, depicting all possible combinations between the considered input factors were framed into an organized design matrix for executing the optimization. Developing regression models for output response predictions is another benefit of using the RSM [191]. Polynomial models of quadratic and cubic orders were formulated through Design Expert and expressed in equations 52 and 53, respectively. Here, *y* represents the response, and x_i represents the factors [192]. *n* denotes the parameter index and β represents the regression coefficient.

$$y = \beta_0 + \sum_{i=1}^{n} \beta_i x_i + \sum_{i=1}^{n-1} \sum_{j=i+1}^{n} \beta_{ij} x_i x_j + \sum_{i=1}^{n} \beta_{ii} x_i^2 \quad (52)$$

$$y = \beta_0 + \sum_{i=1}^{n} \beta_i x_i + \sum_{i=1}^{n-1} \sum_{j=i+1}^{n} \beta_{ij} x_i x_j + \sum_{i=1}^{n} \beta_{ii} x_i^2 + \sum_{i=1}^{n} \beta_{iii} x_i^3 \quad (53)$$

The desirability-function approach was considered for the optimization. Thus, the RSM-optimizer solution characterizing maximum composite desirability value is announced as the optimal solution in all the executed RSM-based analysis works in the result[193]. Concerning the statistical-based RSM-generated regression modelling, the discrepancy between the statistically expected and the actual outputs are represented through residuals. To determine whether the residuals deviate from random distribution (normalcy), normal probability plots were used[194]. A perfectly normally distributed residual is indicated by the red line. As all output response residuals were found to closely match the normality, the corresponding regression models could effectively trace the actual simulation results [195]. The small observed discrepancies could likely result from the ineffectiveness of the regression models in tracing higher-order terms accurately.

By the desirability approach, executing the optimization via the RSM strategy seeks to maximize the combined overall desirability function (*D*). *D* is a function of individual

desirability (*d*) levels with respect to their relative importance (r_i). The *d* is further dependent upon defined goals, the upper and lower limits, with their weights (*w*, set according to the goals) [196-198]. Correlations for devising *d* and *D* functions using the response value (*Y*), parameter upper limit (*U*), lower limit (*L*), and with defined importance levels (*i*) of the goal have been represented in equations 54 and 55.

$$d_i = \begin{cases} 1 \text{ if } Y_i > U_i \\ \left(\dfrac{Y_i - L_i}{U_i - L_i} \right)^w \text{ if } L_i \le Y_i \le U_i \\ 0 \text{ if } Y_i < U_i \end{cases} \tag{54}$$

$$D = \left({d_1}^{r_1} . {d_2}^{r_2} . {d_3}^{r_3} .... {d_m}^{r_m} \right)^{\left(\frac{1}{\sum r_i} \right)} \tag{55}$$

Table 3.7 acts as a sample and depicts the set optimization constraints in Design Expert 13 toward generating the most feasible optimization goals (possessing the highest overall/cumulative desirability) among all the cases of optimization corresponding to the first case of investigation studies incorporated into the thesis work (that is, section 4.1 in the results). The tabulation also incorporates the parametric upper and lower limits and levels and importance assigned for each parametric goal. The optimization results are constrained to 'Units' considered for modelling. Accordingly, the RSM operations were executed. For instance, for the case of efficiency improvement study at the stoichiometric burn case of the blended fuels, the engine efficiency parameters (ITE, BTE) were allotted greater significance. As efficiency improvement constrains higher power outputs[113], the IP and BP were assigned low optimization importance. Besides this, the BSEC and emissions (CO and NO) were assigned an average importance of 3.

Table 3.7: Optimizer Constraints

Parameters	Units	Goal	Lower limit	Upper Limit	Regression order	Importance
Inputs:						
SSPG	%	in range	5	75	-	3
LIVC	º ABDC	in range	50	90	-	3
SOI	º BTDC	in range	30	50	-	3
Output:						
ITE	%	maximize	29.95	37.38	Quadratic	4
IP	kW	maximize	3.85	6.14	Quadratic	1
BTE	%	maximize	22.06	28.38	Quadratic	4
BP	kW	maximize	2.756	5.05	Quadratic	1
BSEC	MJ/kWh	minimize	12.668	16.811	Cubic	3
CO	% V.	minimize	0.58	1.01	Cubic	3
NO	ppm	minimize	711.5	3951.2	Cubic	3

Furthermore, the schematic for the overall investigation approach for inspection and analysis of any performance improvement strategy has been presented in Figure 3.2.1. The optimization operation is majorly oriented toward efficiency improvement to effectively exploit the LIVC-miller cycle strategy. But, better performance and low emission outputs also needed to be tartaned. Thus, multi-objective optimization was performed[191]. The design of experiments (DoE) strategy was employed through RSM-strategy to perform the optimization through fewer iterative efforts[199], besides saving time and reducing computations to predict the optimum [163]. A schematic of the RSM approach for multi-objective optimization is depicted in Figure 3.2.2.

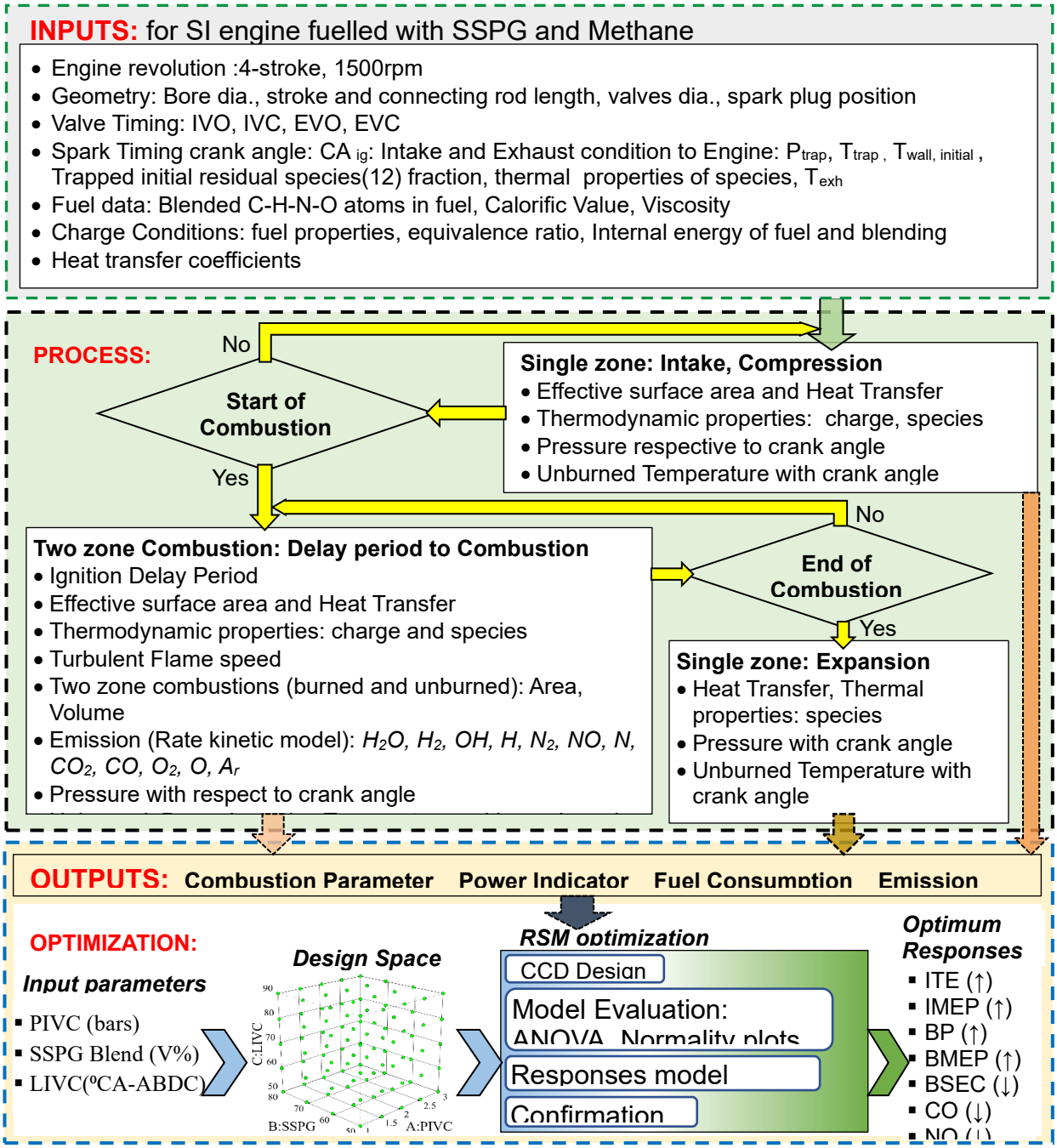

Figure 3.2.1. Engine simulation and optimization procedure layout

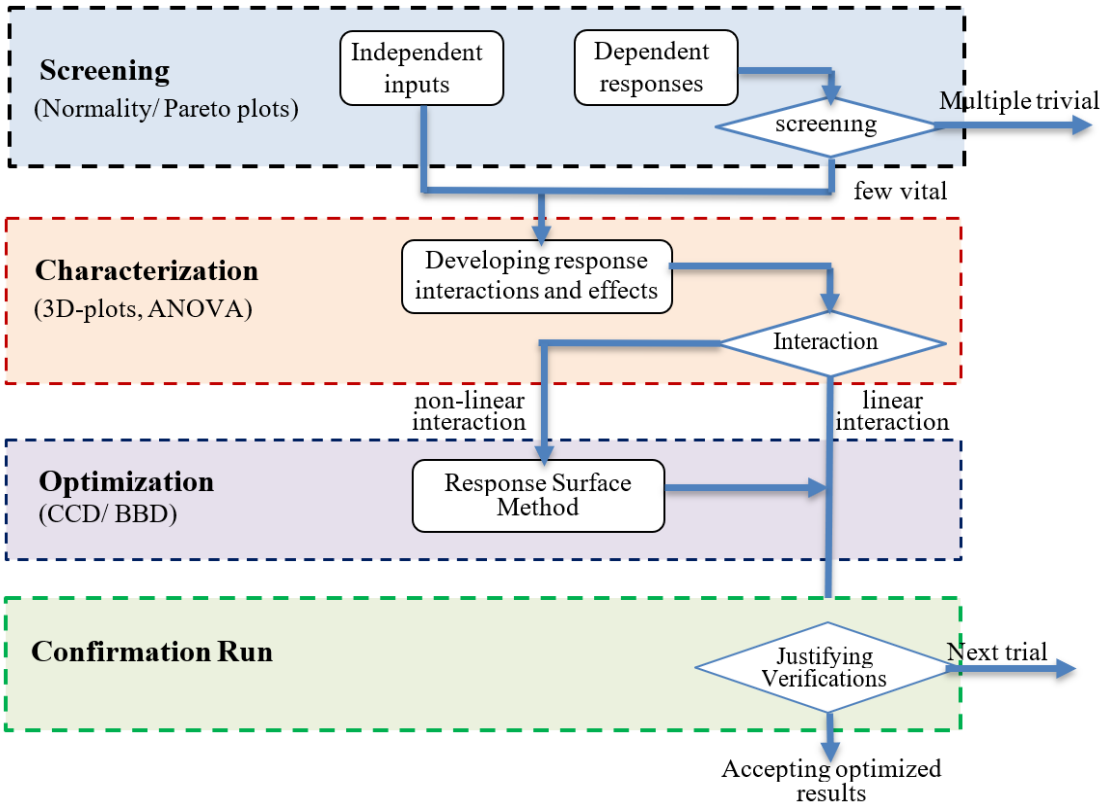

Figure 3.2.2. RSM-based optimization layout